The Astrophysical Journal, 991:34 (9pp), 2025 September 20 https://doi.org/10.3847/1538-4357/adf4c0

Are Local Group Dwarf Spheroidal Galaxies the First Safe Planet-hosting Environments?

Stefano Ciabattini[1,2], Stefania Salvadori[1,2], and Leonardo Testi[2,3]
[1] Dipartimento di Fisica e Astrofisica, Universitá degli Studi di Firenze, Via G. Sansone 1, 50019 Sesto Fiorentino, Italy; stefano.ciabattini@unifi.it
[2] INAF/Osservatorio Astrofisico di Arcetri, Largo E. Fermi 5, 50125 Firenze, Italy
[3] Alma Mater Studiorum, Universitá di Bologna, Dipartimento di Fisica e Astronomia (DIFA), Via Gobetti 93/2, 40129 Bologna, Italy
Received 2025 March 17; revised 2025 July 11; accepted 2025 July 25; published 2025 September 12

Abstract

We explore whether Local Group dwarf spheroidal (dSph) galaxies might have hosted Earth-like planets dwelling unexposed for several billions of years to major galactic threats to life, such as supernovae and gamma-ray bursts. To this aim, we developed a novel semiempirical model that exploits the observed chemical abundances and star formation histories of a selected sample of local dSphs, to explore whether their stars may have (i) reached the minimum metallicity to trigger planet formation and (ii) avoided exposure to destructive events long enough to provide time for possible biological development. From our work two scenarios emerge. If planet formation is possible for [Fe/H] $\lesssim -1$, then in all dSphs with $5 \times 10^3\,L_\odot \leqslant L_V \leqslant 2 \times 10^7\,L_\odot$ a fraction ≈0.1%–10% of stars might have safely hosted terrestrial planets for more than 1 Gyr. In this scenario, ancient ultrafaint dwarf galaxies (UFDs, $L_V \leqslant 10^5\,L_\odot$) would have been the first to reach this condition in the history of the Local Group. Conversely, if planets form for [Fe/H] $\geqslant -0.6$ then they should not exist in UFDs, while only ≈0.001%–0.1% of stars in dSphs with $L_V \geqslant 3 \times 10^5\,L_\odot$ would host planets dwelling in safe conditions for long times. Interestingly, we find a "luminosity sweet spot" at $L_V \sim 10^6\,L_\odot$, where dSphs in our sample safely host terrestrial planets up to 4 Gyr and in any planet formation scenario explored. In conclusion, planet formation at low metallicity is key to understanding which types of galaxies might have formed Earth-like planets that dwelt unexposed to galactic threats over several billions of years, first in the history of the Local Group.

Unified Astronomy Thesaurus concepts: Dwarf galaxies (416); Planet formation (1241); Galaxy evolution (594); Astrobiology (74)

1. Introduction

Habitability is generally associated with the stellar habitable zone, i.e., the region around a star where liquid water can exist on the surface of a terrestrial (i.e., Earth-like) planet for an extended period of time (e.g., S.-S. Huang 1959; J. F. Kasting et al. 1993; R. K. Kopparapu et al. 2013). Hence, such a concept is linked to the scale of a single-planetary system. However, G. Gonzalez et al. (2001) for the first time considered habitability on a larger scale, extending the idea to the entire Milky Way (MW). In particular, they identified a region of the Galaxy that is sufficiently enhanced in heavy elements to form terrestrial planets, which could provide a long-term habitat for life. For this reason, the minimum metallicity to trigger planet formation is considered a key quantity to determine the probability of potentially habitable planetary systems to form in a galaxy.

Still, this is just one of the two necessary (but not sufficient) conditions to potentially form a life-suitable planet. Indeed, catastrophic events occurring during the evolution of a galaxy, such as supernova (SN) explosions, gamma-ray bursts (GRBs), accreting black holes, and merging of compact objects, might represent a serious risk to life on a planet (e.g., M. A. Ruderman 1974; W. H. Tucker 1981; N. Gehrels et al. 2003; A. L. Melott & B. C. Thomas 2011). These events, in fact, inject a large amount of energy into their surroundings and could have a severe impact on the habitability of nearby Earth-like planets. Based on these arguments, different studies have used galactic chemical evolution models to estimate the probability of habitable planets to form and evolve safely from life-harmful events, in our own Galaxy (e.g., C. Lineweaver et al. 2004; N. Prantzos 2008; E. Spitoni et al. 2014, 2017; R. Spinelli et al. 2021) or even in other massive galaxies (e.g., E. Spitoni et al. 2014; P. Dayal et al. 2015).

However, the standard cosmological model predicts that massive galaxies such as the MW are built through the assembling of low-mass progenitor dwarf galaxies, formed at earlier cosmic epochs (e.g., H. J. Mo & S. D. M. White 2002; A. Helmi 2008; S. Salvadori et al. 2015). Some of these ancient dwarf galaxies are not incorporated into the main central object and evolve through cosmic time as satellites. In the Local Group (LG) there are ∼100 known satellite dwarf galaxies (A. B. Pace 2024). Among them, the so-called dwarf spheroidal (dSph) galaxies host >10 Gyr ancient and metal-poor stellar populations, and are currently lacking gas and star formation (e.g., E. Tolstoy et al. 2009). DSph galaxies span several orders of magnitude in luminosity and stellar mass: from ultrafaint dSphs (UFDs, $M_\star \approx 10^{3-5}\,M_\odot$, e.g., J. D. Simon 2019) to brighter "classical" dSphs ($M_\star \approx 10^{5-7}\,M_\odot$, e.g., A. W. McConnachie 2012).

In this work we explore whether and when LG dSph galaxies might have formed stars equipped with terrestrial planets that remained safe from destructive events during galaxy evolution. In particular, we aim at addressing the following questions: Did LG dSph galaxies develop the conditions to potentially host life in the very early Universe? And if so, when did UFDs and "classical" dSphs meet these conditions? To address these issues we develop a novel semiempirical model that exploits the large amount of

Table 1
Observed Properties of dSph Galaxies from R. R. Muñoz et al. (2018) and the SAGA Database

Galaxy	$\log(L_V/L_\odot)$	$R_{1/2}$ (pc)	$\langle[Fe/H]_*\rangle$	N_*^{obs}
Coma Berenices (Com)	3.682	72.6	−2.49	9
Leo IV	3.930	117	−2.35	5
Ursa Major I (UMa I)	3.981	234	−1.98	17
Canes Venatici II (CVn II)	4.002	70.7	−2.07	8
Hercules (Her)	4.266	224	−2.21	26
Boötes I (Boo I)	4.338	202	−2.47	76
Draco (Dra)	5.417	212	−1.88	340
Ursa Minor (UMi)	5.546	404	−1.97	224
Carina (Car)	5.706	311	−1.41	1027
Sculptor (Scl)	6.262	311	−1.80	608
Fornax (For)	7.317	791	−1.06	1608

public-available data, for both the star formation histories (SFHs) and stellar chemical abundances of LG dSphs.

2. The Data Sample

To estimate the probability that a galaxy can safely host terrestrial planets we need to know both the metallicity distribution function (MDF) and the SFH of its stellar populations. Therefore, our dSph sample includes 11 galaxies for which these two pieces of information are simultaneously available from the literature. In particular, we have six UFDs and five classical dSphs, whose names and observed properties are reported in Table 1. Note that the dSphs in our sample span ≈4 orders of magnitude in total luminosity (L_V). We also report the half-light radius of the dSphs, $R_{1/2}$, which is estimated as the scale length of the exponential profile used by R. R. Muñoz et al. (2018) to fit the observed surface brightness of the galaxy. Note that $R_{1/2}$ tends to increase for brighter dSphs. Finally, for each dSph we report the average iron abundance of the stars, $\langle[Fe/H]_*\rangle$, and the number of stellar [Fe/H] measurements, N_*^{obs}.

2.1. MDFs

The MDFs of nearby dSph galaxies are obtained by measuring the iron abundance of their individual stars through spectroscopic observations (e.g., E. N. Kirby et al. 2008). Here we aim to build MDFs using data as consistent as possible; thus, we retrieved the [Fe/H] measurements for stars in dSphs in our sample via the SAGA database (T. Suda et al. 2008). After selecting the most recent work for stars with multiple measurements, we ended up with a sample of 3965 stars with measured [Fe/H] in total. We corrected these measurements for the effects of 1D non–local thermodynamic equilibrium (NLTE), using the online tool `NLiTE` (I. Koutsouridou et al. 2025). For each dSph the corrected average iron abundance is reported in Table 1. The MDFs of UFDs and classical dSphs obtained from this sample of measurements are shown in the left panels of Figure 1. We can see that, despite being dominated by very metal-poor stars, UFDs feature an extremely broad MDF, which extends up to [Fe/H] ∼ −1. For more luminous dSphs the peak of the MDF is located at increasing [Fe/H].

2.2. SFHs

SFHs of nearby dSph galaxies are obtained from their observed color–magnitude diagrams combined with the chemical properties of their stars (e.g., E. Tolstoy et al. 2009). In order to have a sample of SFHs as consistent as possible, we used those from T. M. Brown et al. (2014) for UFDs, and those from D. R. Weisz et al. (2014) for classical dSphs. Both works obtained SFHs for individual galaxies by simultaneously fitting the color–magnitude diagrams from Hubble Space Telescope observations and the stellar metallicity with stellar population models. Furthermore, both provided the SFHs as the cumulative stellar mass fraction formed in each galaxy versus the stellar age, which we converted here into lookback time.

In the right panels of Figure 1 we show the cumulative mass fraction of stars formed in dSphs at different cosmic times (T. M. Brown et al. 2014; D. R. Weisz et al. 2014; solid curves). We see that all UFDs show a similar evolution: they form the bulk of their stars at early times and then are rapidly quenched, >75% of present-day stars being ≳13 Gyr old (see also T. M. Brown et al. 2014). On the other hand, more luminous dSphs have longer and diversified SFHs, some with a major phase of star formation followed by minor activity until a few Gyr ago (e.g., Dra, UMi, and Scl), others with alternating epochs of star formation and quiescence (e.g., Car). Hence, these classical dSphs host stellar populations with a variety of ages, all of them also including ≈13 Gyr old stars.

3. The Model

In our semiempirical model, we compute the probability that LG dSph galaxies might have hosted terrestrial planets dwelling in a safe environment as

$$P_{host} = P_{form} \times P_{surv}, \quad (1)$$

where P_{form} is the probability of dSphs forming terrestrial planets, and P_{surv} the probability of planets in dSphs to survive life-harmful galactic events for a time Δt. These two probabilities are respectively defined by exploiting the observed MDFs and SFHs of dSph galaxies (see Sections 3.1 and 3.3). Note that our model focuses on dSphs because we want to understand whether these ancient systems might have been the first to host planets in such conditions. However, our model is general and thus potentially applicable to any system with an available MDF and SFH.

3.1. Formation of Terrestrial Planets

We evaluate the probability of formation of terrestrial planets around stars in local dSphs as

$$P_{form} = \frac{1}{N_{*,tot}} \sum_i f_{TP}([Fe/H]) N_*([Fe/H]_i) \quad (2)$$

where $N_*([Fe/H]_i)$ is the number of stars in the ith [Fe/H] bin of the MDF, $N_{*,tot}$ is the total number of stars with measured [Fe/H] in the dSph, and $f_{TP}([Fe/H])$ is the probability of terrestrial planets formation as a function of the stellar [Fe/H].

Theoretical predictions for the minimum metallicity to trigger planet formation vary significantly in the literature. In this work we start by assuming the simplest shape for $f_{TP}([Fe/H])$, i.e., a flat distribution above a minimum [Fe/H] (F# models) as shown in Figure 2:

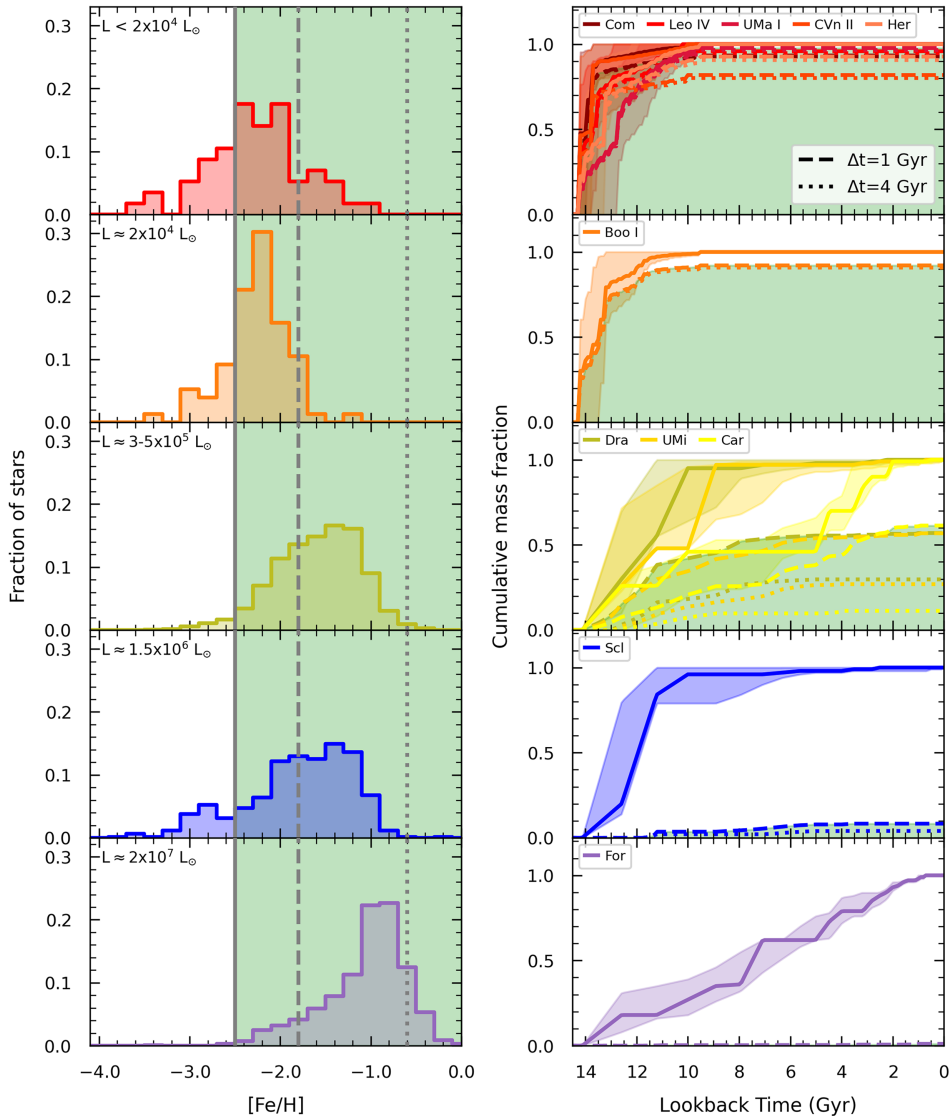

Figure 1. The MDFs (left) and the SFHs (right) of dSphs with increasing luminosity from top (red) to bottom (violet—see also labels). Left panels: all [Fe/H] measurements of stars in dSphs are taken from the SAGA database (http://sagadatabase.jp/) and have been corrected for 1D NLTE effects with the `NLiTE` tool (I. Koutsouridou et al. 2025). Vertical lines represent the minimum [Fe/H] for planet formation in models F1 and E1 (solid), F2 (dashed), and F3 and E2 (dotted; see also Section 3.1). The green shaded areas highlight the [Fe/H] $\geqslant -2.5$ regime. Right panels: as a function of time we show the cumulative mass fraction of stars that (i) are formed in each dSph (solid lines with 1σ uncertainties, data from T. M. Brown et al. 2014 and D. R. Weisz et al. 2014) and (ii) evolve in nonsterilized regions for 1 Gyr (dashed) and 4 Gyr (dotted)—both highlighted with green shaded areas.

1. [Fe/H] $\geqslant -2.5$ (J. L. Johnson & H. Li 2012, model F1)
2. [Fe/H] $\geqslant -1.8$ (Y. Hasegawa & H. Hirashita 2014, F2)
3. [Fe/H] $\geqslant -0.6$ (G. Andama et al. 2024, F3)

Moreover, we explore two additional models that account for the metallicity-dependent occurrence rate of small-period (<10 days) terrestrial planets, recently observed around FGK stars in the MW (J. K. Zink et al. 2023; K. M. Boley et al. 2024). The observed trends have been extrapolated to lower [Fe/H] (E# models) and they are shown in Figure 2. We see that the E# models decline with decreasing [Fe/H] by following

1. a power law (J. K. Zink et al. 2023, E1)
2. an exponential law (K. M. Boley et al. 2024, E2)

In Figure 2 the probabilities of all these models for terrestrial planets formation are reported as a function of the iron abundance of the hosting star and are normalized to reproduce the observed occurrence rate of terrestrial planets at [Fe/H] $= 0$, i.e., $f_{\rm TP} = 0.14$ (K. M. Boley et al. 2024). Note that $f_{\rm TP} = 0$ below each minimum [Fe/H] for models F1–F3, while in E1 $f_{\rm TP}$ is extrapolated down to [Fe/H] $= -2.5$, and in E2 $f_{\rm TP} < 10^{-5}$ for [Fe/H] ~ -0.8.

3.2. Galactic Sources of Sterilization

In principle, the emission from a nearby SN or GRB could induce ozone depletion in the Earth's atmosphere, so that life on the surface would be exposed to deadly doses of solar UV light, and possibly go extinct (e.g., M. A. Ruderman 1974; S. E. Thorsett 1995). Here, we compute the volume sterilized by a single source as

$$V_{\rm ster} = \frac{4\pi}{3} d_{\rm cr}^3 \left(1 - \cos\frac{\theta}{2}\right), \tag{3}$$

where d_{cr} is the maximum distance up to which the source emission could destroy life on a planet, and θ takes into account the geometry of the emission. In the case of Type II SNe (SNe II) we adopt $d_{cr} = 14$ pc, accounting for both standard (N. Gehrels et al. 2003; A. L. Melott & B. C. Thomas 2011; B. Fields et al. 2020) and strong X emission[4] (I. R. Brunton et al. 2023) SNe II, while for Type Ia SNe (SNe Ia) we estimate $d_{cr} \approx 100$ pc based on observational data from E. Churazov et al. (2015) (for details see Appendix B). We set $\theta = \pi$ for all SNe (spherical symmetry). Finally, for GRBs we adopt $d_{cr} = 1$ kpc (B. C. Thomas et al. 2005a, 2005b) and $\theta = 10°$ in order to take into account their typical collimation (see A. Goldstein et al. 2016).

3.3. Sterilization-free Environments

In this section we show how we compute P_{surv}, defined as the probability of terrestrial planets in dSphs to survive galactic threats long enough to allow possible biological development. First, we convert the cumulative SFH into a star formation rate (SFR) as a function of time, adopting a mass-to-light ratio $M/L = 1$ and a time step[5] of 100 Myr. Assuming that stars are homogeneously distributed within the volume of the dSphs, we compute the stellar mass fraction that forms at a time t and that is unaffected by sterilizing effects of galactic sources (see Section 3.2) between t and $t + \Delta t$:

$$f_{surv}(t, \Delta t) = \frac{M_*(t)}{M_*^{tot}}\left(1 - \frac{V_{fill}(t, \Delta t)}{V_{gal}}\right), \quad (4)$$

where $M_*(t)$ is the stellar mass formed at t, M_*^{tot} is the total stellar mass observed today, and $V_{gal} = (4\pi/3)R_{gal}^3$ is the volume of the galaxy with $R_{gal} = 2R_{1/2}$. The quantity $V_{fill}(t, \Delta t)$ is the dSph volume affected by lethal emission between t and $t + \Delta t$, and is computed as

$$V_{fill}(t, \Delta t) = \sum_j V_{ster,j} \int_t^{t+\Delta t} R_j(t')dt', \quad (5)$$

where $V_{ster,j}$ is the volume sterilized by the jth source (SN II, SN Ia, or GRB) from Equation (3), and $R_j(t')$ is the rate of the jth source at time t' computed using analytic prescriptions (see Appendix A for details). If $V_{fill}(t, \Delta t) > V_{gal}$ all stars (and planets) that form at t are bathed by lethal emission between t and $t + \Delta t$, then $f_{surv}(t, \Delta t) \equiv 0$. Note that Equation (5) overestimates $V_{fill}(t, \Delta t)$, as the regions sterilized by different sources could partially overlap. Consequently, Equation (4) might underestimate $f_{surv}(t, \Delta t)$. We integrate Equation (5) for both the timescales typically assumed for the appearance of life on Earth in its embryonic form ($\Delta t = 1$ Gyr) and its evolution into an intelligent one ($\Delta t = 4$ Gyr).

Finally, by integrating Equation (4) between the time at which the dSph galaxy begins forming stars (t_{form}) and the present day (t_{today}), we get the global mass fraction of stars that are not irradiated from any galactic source at a distance $d < d_{cr}$ for a time Δt. We interpret this as P_{surv}, i.e., the probability of putative terrestrial planets in the dSph to survive sterilizing effects from nearby galactic sources for a time Δt:

$$P_{surv} = \int_{t_{form}}^{t_{today}} f_{surv}(t', \Delta t)dt'. \quad (6)$$

Note that, for a given SFH, the value of P_{surv} changes when adopting a different Δt.

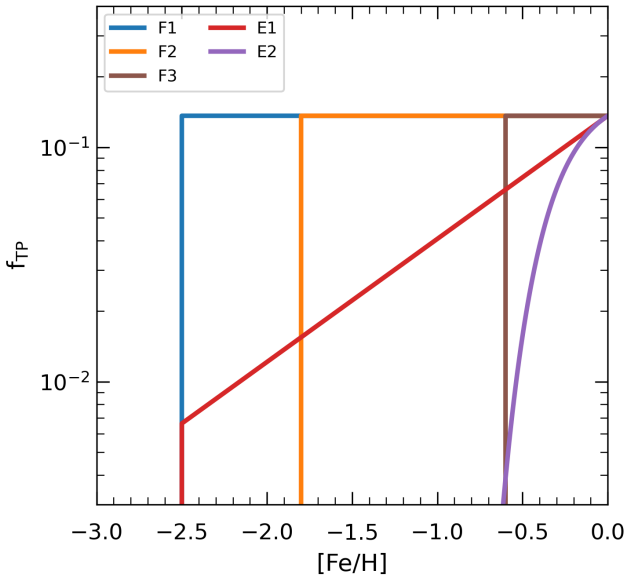

Figure 2. Adopted metallicity-dependent probabilities terrestrial planets formation. See labels and text for the different models assumed.

4. Results

In this section, we present the results of our model, starting with those reported in the right panel of Figure 1. Here we show, for dSph galaxies with different luminosities, the cumulative mass fraction of stars that survive life-harmful events for a time Δt, obtained by integrating Equation (4). The area below each curve is highlighted in green. First, we see that these cumulative fractions decrease with the luminosity of the dSphs. In particular, in all UFDs the majority of stars contribute to the cumulative f_{surv}, which is already >80% of the total around 9 Gyr ago and independent of the assumed Δt. In more luminous classical dSphs, this fraction is initially zero, it remains ⩽60% for dSphs with intermediate luminosities (if $\Delta t = 1$ Gyr), and it reaches the minimum for the brightest dSph galaxy, Fornax.

These results can be explained as follows: the higher the luminosity of a dSph (and so the higher its final stellar mass) the higher its SFR[6] and in turn the rate of disruptive events, resulting in a larger sterilized volume fraction (see Equations (5), (A1), and (A3)).

Note that in dSphs with intermediate luminosity (Dra, UMi, and Car) the choice of Δt can strongly affect the fraction of stars that contribute to f_{surv}. The effect is particularly evident in Carina, which has a peculiar SFH made up of two main bursts of star formation, the last and more intense one occurring <4 Gyr ago. We should also note that, despite the different luminosities, all UFDs show similar (cumulative) values of f_{surv}. This is due to their peculiar SFH. Since almost all stars in UFDs formed in the first billion years of cosmic evolution, the

[4] These only represent 7% of the whole SN II population (W. Li et al. 2011; C. Cold & J. Hjorth 2023).

[5] Assuming different time steps does not affect our findings.

[6] SFR $< 10^{-4}\,M_\odot\,\mathrm{yr}^{-1}$ in UFDs while SFR $\approx (10^{-4}$–$10^{-3})\,M_\odot\,\mathrm{yr}^{-1}$ in classical dSphs; see also S. Salvadori et al. (2014).

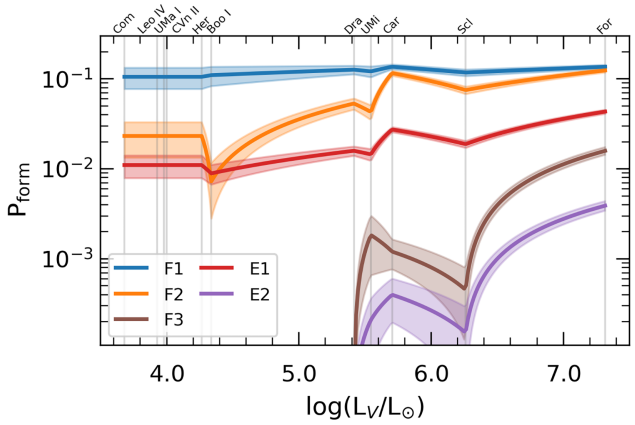

Figure 3. Probability of formation of terrestrial planets in local dSphs, $P_{\rm form}$, as a function of the dSph luminosity. Each curve corresponds to a specific model for $f_{\rm TP}$ (see labels and Figure 2), and is the linear interpolation of values computed for dSphs in our sample (identified by vertical lines). Shaded areas represent the uncertainties.

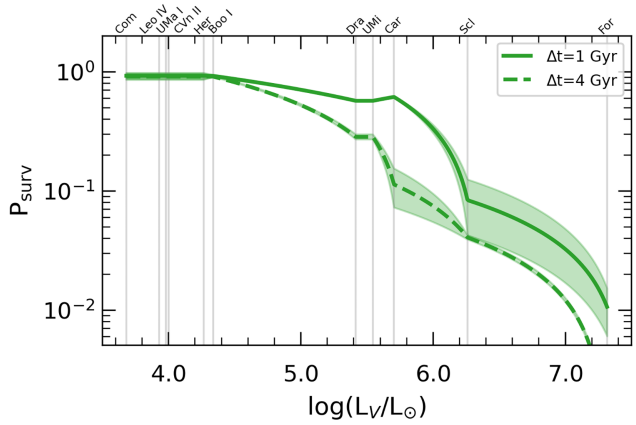

Figure 4. Probability of putative planets in local dSphs to survive, for a time Δt, against destructive galactic events, $P_{\rm surv}$, as a function of the dSph luminosity. Curves are obtained as the linear interpolation of the values computed for dSphs in our sample (identified by vertical lines), in the cases of $\Delta t = 1$ Gyr (solid) and $\Delta t = 4$ Gyr (dashed). Shaded areas represent the uncertainties.

rate of SNe and GRBs in these galaxies rapidly drops ∼30 Myr after[7] the quenching of star formation. Furthermore, the contribution of SNe Ia is negligible because of the low SFR in UFDs. Ultimately, the total number of destructive events in UFDs is limited in size and time. Thus, only a small portion of the galaxy is sterilized and more than 80% of the stars that formed in the UFD during the first billion years of cosmic evolution are hosted in a galactic environment free from destructive events, up to the present day.

4.1. Terrestrial Planets in LG dSphs

In Figure 3 we show the probability of formation of terrestrial planets around stars in local dSphs, $P_{\rm form}$, as a function of the dSph's luminosity, L_V. The five curves show the results obtained by assuming different $f_{\rm TP}$([Fe/H]) (see Section 3.1). Each curve is the linear interpolation between the values of $P_{\rm form}$ computed for each dSph in our sample. Shaded areas show Poissonian uncertainties, which are lower for higher L_V because of the larger number of available measurements.

In Figure 3 we see that the results can be divided into two groups showing different trends. Models that allow the formation of terrestrial planets around stars with [Fe/H] $\lesssim -1$ and assume a constant (F1, F2) or an increasing (E1) $f_{\rm TP}$ with [Fe/H] yield $P_{\rm form} \approx 1\%$–10% for all dSphs in our sample. In these cases $P_{\rm form}$ is maximum ($\gtrsim$10%) and (almost) independent of L_V for model F1, which assumes $f_{\rm TP} = 0.14$ for [Fe/H] $\geqslant -2.5$, while it increases with L_V and is $\leqslant$10% for both models F2 and E1, which assume different shapes for $f_{\rm TP}$ (see Figure 2 and Section 3.1). In contrast, if terrestrial planets can only form around stars with [Fe/H] $\geqslant -0.6$ (models F3 and E2), then they should not exist in UFDs. This is due to the fact that UFDs are the most metal-poor galaxies, lacking stars at these iron abundance values as shown in the left panels of Figure 1. Note that these models predict $P_{\rm form} < 1\%$ for classical dSphs, with large variations for $L_V \gtrsim 10^{5.4}\,L_\odot$ and the maximum $P_{\rm form}$ reached for the most luminous For dSphs. This is because the MDFs of classical dSphs have a peak increasing with L_V, but they are all poorly populated at [Fe/H] $\geqslant -0.6$.

[7] The lifetime of 8 $M_\odot$ stars is ≈25 Myr (C. M. Raiteri et al. 1996).

Ultimately, two major scenarios emerge for the formation of terrestrial planets in dSphs: (i) they form in both UFDs and classical dSphs with a probability of 1%–10% if $f_{\rm TP} > 0$ for [Fe/H] $\lesssim -1$; (ii) they only form in luminous classical dSphs if $f_{\rm TP} > 0$ for [Fe/H] $\geqslant -0.6$ with a lower probability $P_{\rm form} = 0.01\%$–1%.

4.2. Life-harmful Events in LG dSphs

In Figure 4 we show the probability of newly formed planets in dSphs to survive life-harmful events, $P_{\rm surv}$, as a function of L_V. The two curves correspond to different timescales for possible biological development. Due to similar but scattered values of $P_{\rm surv}$ in UFDs, here we show the average value for all of them, with the only exception of Boötes I. Overall, we see that $P_{\rm surv}$ is roughly constant ($P_{\rm surv} \sim 1$) for $L_V < 10^5\,L_\odot$ (i.e., for UFDs), and then it decreases for increasing L_V down to $P_{\rm surv} \sim 0.01$ (or $P_{\rm surv} = 0$ for $\Delta t = 4$ Gyr) for the Fornax dSph. This decreasing trend can be explained as follows. More luminous dSphs have larger SFRs, yielding higher rates of destructive events; hence, despite being larger than UFDs, they are more significantly affected by life-harmful events, resulting in a lower $P_{\rm surv}$ (see Equations (4) and (6)).

We see that when we consider a longer Δt, we get lower values of $P_{\rm surv}$ for $L_V \gtrsim 10^{4.3}\,L_\odot$. Indeed, with respect to UFDs, more luminous dSphs have more stars, but they are formed on much longer timescales (see the right panels of Figure 1). As a result, the rate of SNe and GRBs is higher and has a much broader distribution in cosmic time.

4.3. Safe Terrestrial Planets in LG dSphs

Figure 5 summarizes the final results of our study, showing the probability of dSphs with different L_V to host safe terrestrial planets, $P_{\rm host}$, for all the different models considered in our study (different $f_{\rm TP}$([Fe/H]) and Δt). Let us start with the left panel, which illustrates the results obtained for $\Delta t = 1$ Gyr, i.e., the timescale for the appearance of life on Earth in its embryonic form. We note once again that the results can be divided into two major groups. In models where planet formation is possible for [Fe/H] $\lesssim -1$ (F1, F2, and E1) $P_{\rm host} \approx 0.8\%$–$10\%$ up to $L_V \simeq 10^{5.7}\,L_\odot$, with small variations

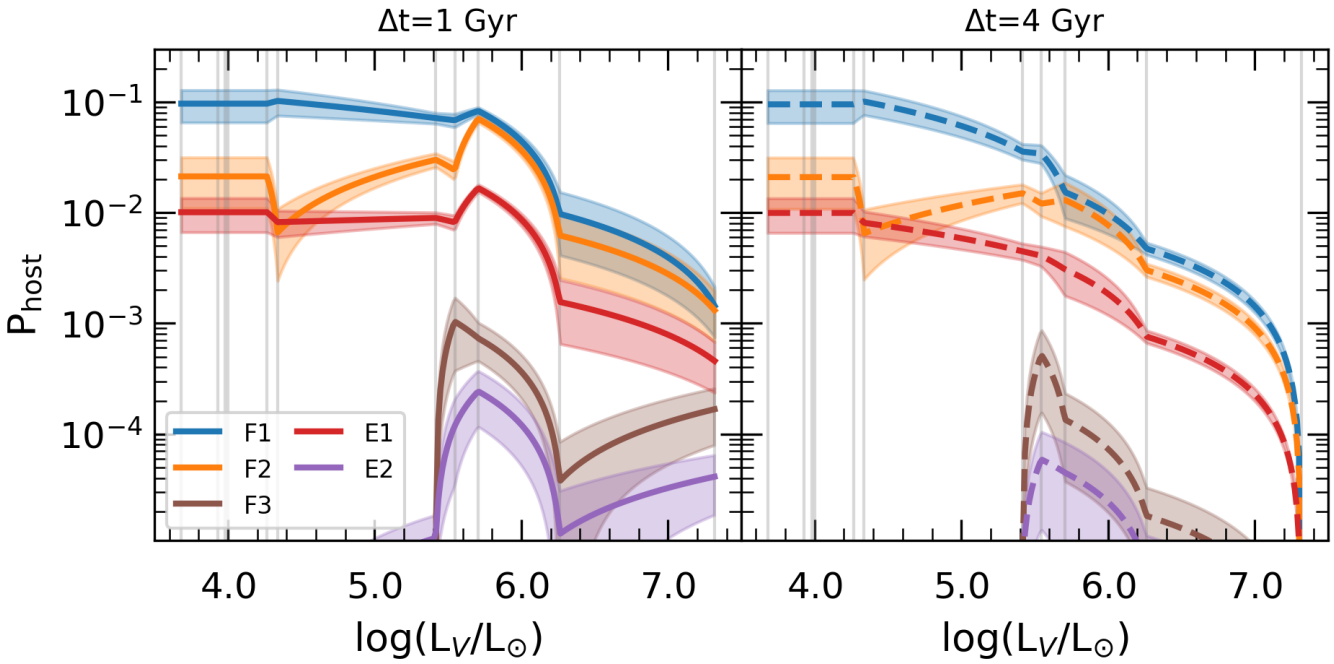

Figure 5. Probability of LG dSphs to host terrestrial planets dwelling for Δt in a safe environment, $P_{\rm host}$, as a function of the dSph luminosity. Curves are obtained through Equation (1), combining $P_{\rm form}$ resulting from different models of $f_{\rm TP}$ (see Figure 3) and $P_{\rm surv}$ for $\Delta t = 1$ Gyr (left panel, solid) and $\Delta t = 4$ Gyr (right panel, dashed). Shaded areas represent the uncertainties from the error propagation in Equation (1).

for each model. For higher L_V it decreases down to $P_{\rm host} \approx 0.04\%$–$0.1\%$ in the Fornax dSph. Conversely, if planets form only for [Fe/H] $\geqslant -0.6$ (models F3 and E2) $P_{\rm host} = 0$ for $L_V < 10^5\,L_\odot$ (hence in all UFDs), while $P_{\rm host} \approx 0.001\%$–$0.1\%$ in more luminous dSphs. When we consider $\Delta t = 4$ Gyr, we obtain similar trends with a few notable differences. While $P_{\rm host}$ is independent of Δt for $L_V \lesssim 10^{4.5}\,L_\odot$, we note that for higher luminosities it assumes lower values with respect to the $\Delta t = 1$ Gyr case. In particular, for dSphs with intermediate L_V (Dra, UMi, and Car) when we assume $\Delta t = 4$ Gyr $P_{\rm host}$ is a factor of $\sim$5 lower, while in the most luminous dSph, Fornax, $P_{\rm host} = 0$. Interestingly, according to our model a sort of "luminosity sweet spot" exists for $10^{5.4}\,L_\odot \leqslant L_V \leqslant 10^{6.6}\,L_\odot$ where $P_{\rm host} > 0$, independently of which $f_{\rm TP}$ or Δt we assume.

Ultimately, our model predicts two possible major scenarios, which are mainly driven by $P_{\rm form}$: (i) if $f_{\rm TP} > 0$ for [Fe/H] $\leqslant -1$, both UFDs and classical dSphs are able to safely host terrestrial planets long enough for possible biological development, with a probability $P_{\rm host} \approx 0.1\%$–$10\%$; (ii) if $f_{\rm TP} > 0$ for [Fe/H] $\geqslant -0.6$, terrestrial planets with possible biological development can only form in classical dSphs and with a much lower probability, $P_{\rm host} \approx 0.001\%$–$0.1\%$.

5. Discussion

In our work we explored the formation of terrestrial planets in LG dSphs, and their long-term galactic exposure to destructive events. Indeed, such planets would represent suitable places in a galaxy for the possible appearance and development of life. However, whether these planets might be actually habitable would also depend on planetary-scale physical aspects, such as the host star's spectral type, planetary orbital distances, and the stellar habitable zone, whose modeling is beyond the scope of this work. Nevertheless, we qualitatively discuss how their interplay might affect our results. Furthermore, we discuss the role of refractory elements (Mg and Si, other than just Fe) in planet formation in metal-poor environments, and consider the possible investigation of other ancient LG environments.

5.1. Stellar Spectral Type and Habitable Zone

The results we used to model $f_{\rm TP}$ are valid only for close-in planets ($\approx$0.01–0.5 au) orbiting FGK stars (see Section 3.1 and references therein). However, the majority of stars in our sample are K and M dwarfs. Indeed, stars with $m \leqslant 0.8\,M_\odot$ belong to the K and M spectral classes (e.g., I. Baraffe et al. 2015), and have lifetimes >9 Gyr (C. M. Raiteri et al. 1996). From the SFHs in Figure 1 we find that all stars in UFDs formed more than 9 Gyr ago, and hence they are K or M. The same argument can be applied to $\geqslant$95% of the stars in Draco, Ursa Minor, and Sculptor, and to $\geqslant$40% of the stars in Carina and Fornax. Thus, in this work, we extend all our models of $f_{\rm TP}$ to M dwarfs and we make a conservative assumption by maintaining the same normalization, despite in the MW the observed planet occurrence rate being higher for M dwarfs (C. D. Dressing & D. Charbonneau 2015; R. Gore et al. 2024) than for FGK stars (J. K. Zink et al. 2023; K. M. Boley et al. 2024). Furthermore, planet formation in low-metallicity environments is expected to occur relatively close to the host star (<0.5 au), as the disk mass is limited (e.g., J. L. Johnson & H. Li 2012). Interestingly, for such close-in planets, it would be possible to orbit within the stellar habitable zone of K and M dwarfs, which for an Earth-like planet includes orbits from $\approx$0.03 au up to $\lesssim$1 au (e.g., R. K. Kopparapu et al. 2013). Ultimately, it would be possible for putative terrestrial planets around K and M dwarfs in local dSph galaxies to orbit within the stellar habitable zone. If so, according to our model these potentially habitable planets would have good chances to evolve in a safe environment from major galactic events, providing a favorable place for life to appear and evolve. To

quantify the probability for life to appear we should model planet formation within the stellar habitable zone as a function of the host star's mass and metallicity. This is beyond the scope of this study, but we plan to do it in a dedicated future work.

5.2. MW Bulge and Globular Clusters

In the LG there are other ancient environments that could be explored in terms of planet formation and long-time exposure to galactic threats, such as the MW bulge and globular clusters (GCs). Despite being more metal-rich (e.g., B. Barbuy et al. 2015), the MW bulge is believed to be inhospitable since early cosmic times because of the high rates of (i) lethal events (R. Spinelli et al. 2021), (ii) ionizing photons emitted by the active galactic nucleus at the center of the MW (A. Ambrifi et al. 2022), and (iii) star formation at early cosmic epochs driven by merging events (G. Pagnini et al. 2023). On the other hand, GCs experience few (or single) bursts of star formation (like UFDs), but their stellar populations have higher [Fe/H] (e.g., D. A. Forbes & T. Bridges 2010; E. Pancino et al. 2017; V. Belokurov & A. Kravtsov 2024). Furthermore, GCs are (1–2) Gyr younger than UFDs (e.g., E. R. Garro et al. 2024) and are expected to host high fractions of X-ray binaries (e.g., M. Bellazzini et al. 1995), which could represent an additional threat to life, and being dense environments their putative planetary systems might be disrupted by stellar encounters (e.g., S. Sigurdsson 1992). Ultimately, investigating GCs as possible sites to safely host terrestrial planets represents an interesting application of our model, although their SFHs suggest that, likely, they would not be the first.

5.3. Refractory Elements

From our study it follows that UFDs might host terrestrial planets only if $f_{\rm TP} > 0$ for [Fe/H] $\lesssim -1$ (see Figure 3). In this regard, we should note that at low [Fe/H] the iron abundance might not be a very good proxy for metallicity. This becomes relevant if we consider that the seeds for planet formation are dust grains (e.g., V. Adibekyan 2019; L. Testi et al. 2022), and that their cores are made of magnesium and silicon, other than iron (e.g., T. Kozasa et al. 1989; P. Todini & A. Ferrara 2001). Indeed, G. Gonzalez (2009) proposed using the refractory index [Ref/H], which accounts for Mg, Si, and Fe, to describe the planet formation probability as a function of metallicity (V. Z. Adibekyan et al. 2012a, 2012b). How does the MDF of UFDs and classical dSphs change when we use [Ref/H] instead of [Fe/H]? And how does it affect our scenarios for planet formation in local dSphs? We selected stars in our sample with [Mg/H], [Si/H], and [Fe/H] high-resolution measurements. Then, we built distributions with respect to each element and [Ref/H]. The results are shown in Figure 6, where we also report the minimum [Fe/H] for which $f_{\rm TP} > 0$ in each model. In each distribution, the red histograms count stars with [Fe/H] < -2.5. We see that in UFDs ≈35% of stars with [Fe/H] < -2.5 have [Ref/H] > -2.5 because of an enhancement in [Mg/H] and/or [Si/H] (while in classical dSphs the increase is less than 1%). Thus, in metal-poor environments such as UFDs, [Fe/H] is not a good proxy for metallicity, and it might lead to an underestimate of the number of planets in metal-poor galaxies. Interestingly, UFDs are known to have the highest fraction of C-enhanced stars (M. Rossi et al. 2023; R. Lucchesi et al. 2024), which are

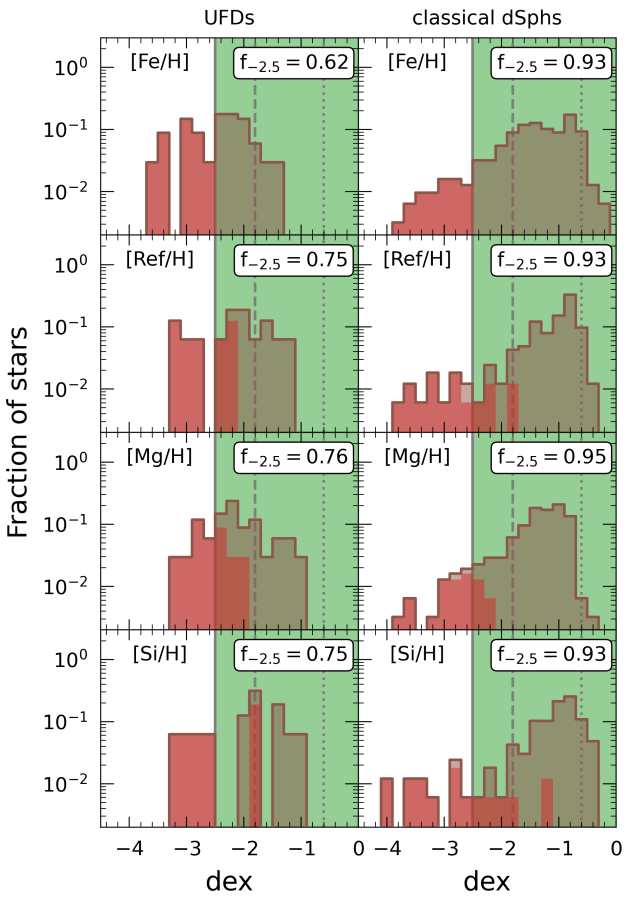

Figure 6. Normalized fraction of stars in UFDs (left) and dSphs (right) with different chemical abundances (see labels) obtained using the high-resolution measurements ($R > 10^4$) in the SAGA database. All measurements are corrected for 1D NLTE effects, using `NLiTE` (I. Koutsouridou et al. 2025). Red histograms show stars with [Fe/H] < -2.5. In each panel we report the fraction of stars above -2.5 dex, $f_{-2.5}$ (see labels). Vertical lines and green shaded areas are the same as those in the left panels of Figure 1.

polluted by the first SNe and thus are also enhanced in Mg and Si (see lower panels of Figure 6; A. Saccardi et al. 2023; I. Vanni et al. 2023). Moreover, recent simulations show that these first SN explosions could have produced an abundant amount of water in their remnants (D. J. Whalen et al. 2025), also inducing the collapse of dense cores where several Earth masses of planetesimals are formed ≈200 Myr after the Big Bang (E. I. Vorobyov et al. 2025).

6. Summary and Conclusion

In this work we explored for the first time whether and when LG dSphs might have hosted terrestrial planets dwelling in a safe galactic environment during their subsequent long-term evolution. To this end, we developed a novel and general semiempirical model that exploits the observed MDFs and SFHs to quantify for each galaxy the probability of forming terrestrial planets around its stars and for putative planets the probability of avoiding life-harmful irradiation from SNe and GRBs, during the expected timescale for life appearance ($\Delta t = 1$ Gyr) and evolution ($\Delta t = 4$ Gyr) on Earth. The model can be applied to every stellar system for which these quantities are measured.

From our model two major scenarios emerge: (i) In models where planet formation is possible for [Fe/H] $\lesssim -1$ (models

F1, F2, and E1), both UFDs and classical dSphs safely host terrestrial planets long enough to possibly allow biological development, with a probability $P_{\rm host} \approx 0.1\%$–$10\%$. (ii) Conversely, if planets form only for [Fe/H] $\geqslant -0.6$ (models F3 and E2), this should be possible only in classical dSphs with $L_V \geqslant 10^{5.4}\,L_\odot$, where $P_{\rm host} \approx 0.001\%$–$0.1\%$. In this case, planets should not exist in UFDs.

Noticeably, in scenario (i) UFDs would be the first local galaxies able to host terrestrial planets in a long-term safe galactic environment, as they form most of their stars during the first billion years of cosmic time, i.e., several billions of years before the formation of our own solar system. In this sense, these ancient and small galaxies we observe today as relics of the early Universe might have become primordial life nurseries.

Skeptics may wonder about the assumptions made in our study. We showed that the choice of a Δt compatible with the timescale of the appearance (1 Gyr) or the evolution (4 Gyr) of life on Earth does not affect the general trends for $P_{\rm host}$, with the two exceptions of the Carina and Fornax dSphs. Furthermore, we checked that the values of $P_{\rm host}$ lie within the uncertainties if we assume a $10\times$ smaller volume for each dSph, i.e., if we mimic an inhomogeneous and more concentrated distribution of stars (see Appendix C).

In conclusion, our work suggests that the minimum metallicity that triggers planet formation around a star and the probability distribution to form planets at different stellar [Fe/H] are key to understanding whether and when this could have happened for the very first time in the history of the LG. Any future search for planets around metal-poor stars (in the MW, but hopefully also in local dSphs) would help us to discriminate between the two scenarios predicted in this work, possibly shedding light on the most ancient systems that could have provided the minimum conditions to potentially host life.

Acknowledgments

The authors want to thank the anonymous referee and the editor for their very constructive comments that have certainly improved this manuscript. S.C. and S.S. acknowledge support by the European Research Council (ERC) Starting Grant NEFERTITI H2020/804240 (PI: Salvadori). L.T. is partly supported by the Italian Ministero dell'Istruzione, Universitá e Ricerca through the grant Progetti Premiali 2012-iALMA (CUP C52I13000140001), the European Union's Horizon 2020 research and innovation program under the Marie Skłodowska-Curie grant agreement No. 823823 (DUSTBUSTERS), and the ERC via the ERC Synergy Grant ECOGAL (grant 855130).

Appendix A
The Rates of SNe II, SNe Ia, and GRBs

Here we describe the analytical relations used to compute the rates of disruptive events in Equation (5). The rate of SNe II is

$$R_{\rm II}(t) = \nu \int_{m_{\rm min}}^{m_{\rm max}} {\rm SFR}(t - \tau(m))\,\phi(m)\,dm \qquad \text{(A1)}$$

where $\phi(m)$ is the initial mass function (IMF), ν is the number of stars per unit stellar mass formed, and $\tau(m)$ is the lifetime of stars with mass m (C. M. Raiteri et al. 1996). We assume $m_{\rm min} = 8\,M_\odot$ and $m_{\rm max} = 40\,M_\odot$—since more massive stars are expected to directly collapse into black holes preventing SN explosion (S. E. Woosley & T. A. Weaver 1995; M. Limongi & A. Chieffi 2018)—and a Larson-type IMF

$$\phi(m) \equiv \frac{dN}{dm} \propto m^{-1+\alpha} \exp\left(-\frac{m_{\rm ch}}{m}\right), \qquad \text{(A2)}$$

in the range [0.1–100] $M_\odot$ with $\alpha = -1.35$ and $m_{\rm ch} = 0.35\,M_\odot$ (R. B. Larson 1998).

For the rate of GRBs, $R_{\rm GRB}(t)$, we use the same Equation (A1) but with $m_{\rm max} = 100\,M_\odot$, and multiply the final value for a factor $f_{\rm GRB} = 0.1$. This accounts for the unknown fraction of massive stars that can originate a GRB either because (i) they are rapidly rotating (long GRBs, e.g., A. I. MacFadyen & S. E. Woosley 1999) or because (ii) they pertain to a binary system in which both companions evolve as compact objects that will later merge (short GRBs, e.g., E. Berger 2014).

For the SN Ia rate we use the relation from F. Matteucci et al. (2006):

$$R_{\rm Ia}(t) = \nu \int_{\tau_{\rm min}}^{\min(t,\tau_{\rm max})} A_{\rm Ia}\,{\rm SFR}(t - \tau)\,{\rm DTD}(\tau)\,d\tau, \qquad \text{(A3)}$$

where DTD(τ) is the delay-time distribution function from F. Mannucci et al. (2006), which accounts for the time needed for an SN Ia to occur after star formation. Following F. Matteucci et al. (2006) we assume that the minimum (maximum) delay time for the occurrence of an SN Ia, $\tau_{\rm min}$ ($\tau_{\rm max}$), is equal to the lifetime of an $8\,M_\odot$ ($0.8\,M_\odot$) star. The quantity $A_{\rm Ia}$ is the fraction of binary systems that produce SNe Ia. In consideration of the lack of constraints for the observed rate of SNe Ia in dSph galaxies, we assume $A_{\rm Ia} = 2.5 \times 10^{-3}$ to reproduce the observed rate of $\approx(0.3/100)$ yr^{-1} in the MW (E. Cappellaro et al. 1999).

Appendix B
Critical Distance for Type Ia SNe

Type Ia SNe emit in the gamma and in principle could induce biological damage on a planet if the time-integrated flux is $\mathcal{F}_\gamma \geqslant \mathcal{F}_\gamma^{\rm cr}$, where $\mathcal{F}_\gamma^{\rm cr} = 10^8$ erg cm^{-2} is the estimated critical value above which there might be lethal consequences for life on Earth (B. C. Thomas et al. 2005a, 2005b; L. M. Ejzak et al. 2007). We exploit available observational data of the SN Ia SN 2014J ($\mathcal{F}_\gamma \approx 7 \times 10^{-2}$ erg cm^{-2}, $d = 3.5$ Mpc; E. Churazov et al. 2015) to estimate the equivalent distance at which the time-integrated flux of SN 2014J would equal the critical value (M. Richmond 2025, private communication), as follows:

$$d_{\rm cr,Ia} = \left(\frac{\mathcal{F}_\gamma}{\mathcal{F}_\gamma^{\rm crit}}\right)^{1/2} d \approx 100\ {\rm pc}. \qquad \text{(B1)}$$

Appendix C
Inhomogeneous Stellar Distribution

Here we discuss how our results change if we assume a radius for the dSph galaxies that is 2 times smaller: $R_{\rm gal} = R_{1/2}$. This mimics an inhomogeneous, but more concentrated, distribution of stars in the dSph galaxies. From the top panels of Figure 7 we see that if we assume $R_{\rm gal} = R_{1/2}$

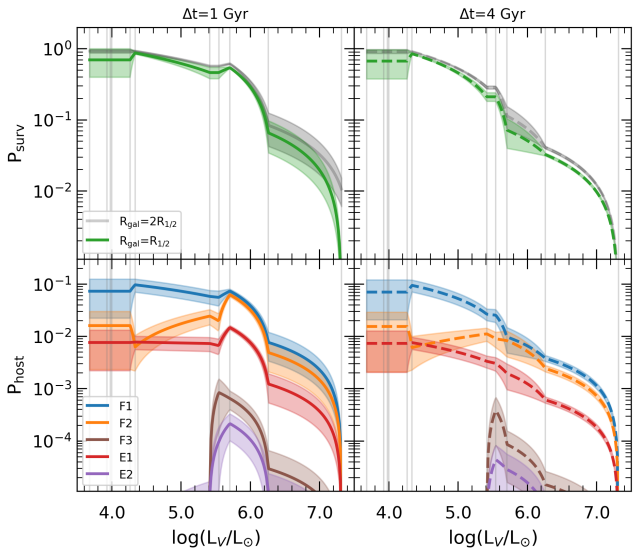

Figure 7. Top: comparison between $P_{\rm surv}$ as a function of L_V, computed for a galaxy radius $R_{\rm gal} = R_{1/2}$ (green) and $R_{\rm gal} = 2R_{1/2}$ (gray, same as Figure 4). Bottom: the curves are the same as those in Figure 5, but obtained using $R_{\rm gal} = R_{1/2}$ for the calculation of $P_{\rm surv}$ (green curves in top panels). Left panels are for $\Delta t = 1$ Gyr (solid curves) and right panels are for $\Delta t = 4$ Gyr (dashed).

(green) the results are roughly consistent with the case of $R_{\rm gal} = 2R_{1/2}$ (gray), for both $\Delta t = 1$ Gyr (in this case with the exception of the Fornax dSph) and $\Delta t = 4$ Gyr. Consequently, since the values of $P_{\rm form}$ have not changed in Equation (1), the same conclusion holds for $P_{\rm host}$ (bottom panels of Figure 7). We note that in UFDs $P_{\rm surv}$ decreases from $\approx 0.90 \pm 0.06$ to $\approx 0.70 \pm 0.30$; however this is solely driven by the two smallest UFDs (Com and CVn II), which have $R_{1/2} \approx 70$ pc and thus can be totally sterilized if the dSph radius is halved. For $L_V \gtrsim 10^{4.3}\, L_\odot$ the difference is $\lesssim$15%. As a consequence, $P_{\rm host}$ decreases for all dSphs too, yet it remains consistent within the uncertainties. We showed that $P_{\rm host}$ lies within the uncertainties if we adopt a 2 times smaller $R_{\rm gal}$.

ORCID iDs

Stefano Ciabattini https://orcid.org/0009-0000-3803-786X
Stefania Salvadori https://orcid.org/0000-0001-7298-2478
Leonardo Testi https://orcid.org/0000-0003-1859-3070

References

Adibekyan, V. 2019, Geosc, 9, 105
Adibekyan, V. Z., Delgado Mena, E., Sousa, S. G., et al. 2012a, A&A, 547, A36
Adibekyan, V. Z., Sousa, S. G., Santos, N. C., et al. 2012b, A&A, 545, A32
Ambrifi, A., Balbi, A., Lingam, M., Tombesi, F., & Perlman, E. 2022, MNRAS, 512, 505
Andama, G., Mah, J., & Bitsch, B. 2024, A&A, 683, A118
Baraffe, I., Homeier, D., Allard, F., & Chabrier, G. 2015, A&A, 577, A42
Barbuy, B., Friaça, A. C. S., da Silveira, C. R., et al. 2015, A&A, 580, A40
Bellazzini, M., Pasquali, A., Federici, L., Ferraro, F. R., & Pecci, F. F. 1995, ApJ, 439, 687
Belokurov, V., & Kravtsov, A. 2024, MNRAS, 528, 3198
Berger, E. 2014, ARA&A, 52, 43
Boley, K. M., Christiansen, J. L., Zink, J., et al. 2024, AJ, 168, 128
Brown, T. M., Tumlinson, J., Geha, M., et al. 2014, ApJ, 796, 91
Brunton, I. R., O'Mahoney, C., Fields, B. D., Melott, A. L., & Thomas, B. C. 2023, ApJ, 947, 42
Cappellaro, E., Evans, R., & Turatto, M. 1999, A&A, 351, 459
Churazov, E., Sunyaev, R., Isern, J., et al. 2015, ApJ, 812, 62
Cold, C., & Hjorth, J. 2023, A&A, 670, A48
Dayal, P., Cockell, C., Rice, K., & Mazumdar, A. 2015, ApJ, 810, L2
Dressing, C. D., & Charbonneau, D. 2015, ApJ, 807, 45
Ejzak, L. M., Melott, A. L., Medvedev, M. V., & Thomas, B. C. 2007, ApJ, 654, 373
Fields, B., Melott, A., Ellis, J., et al. 2020, PNAS, 117, 21008
Forbes, D. A., & Bridges, T. 2010, MNRAS, 404, 1203
Garro, E. R., Minniti, D., & Fernández-Trincado, J. G. 2024, A&A, 687, A214
Gehrels, N., Laird, C. M., Jackman, C. H., et al. 2003, ApJ, 585, 1169
Goldstein, A., Connaughton, V., Briggs, M. S., & Burns, E. 2016, ApJ, 818, 18
Gonzalez, G. 2009, MNRAS, 399, L103
Gonzalez, G., Brownlee, D., & Ward, P. 2001, Icar, 152, 185
Gore, R., Giacalone, S., Dressing, C. D., et al. 2024, ApJS, 271, 48
Hasegawa, Y., & Hirashita, H. 2014, ApJ, 788, 62
Helmi, A. 2008, A&ARv, 15, 145
Huang, S.-S. 1959, PASP, 71, 421
Johnson, J. L., & Li, H. 2012, ApJ, 751, 81
Kasting, J. F., Whitmire, D. P., & Reynolds, R. T. 1993, Icar, 101, 108
Kirby, E. N., Simon, J. D., Geha, M., Guhathakurta, P., & Frebel, A. 2008, ApJ, 685, L43
Kopparapu, R. K., Ramirez, R., Kasting, J. F., et al. 2013, ApJ, 765, 131
Koutsouridou, I., Skúladóttir, Á., & Salvadori, S. 2025, A&A, 699, A32
Kozasa, T., Hasegawa, H., & Nomoto, K. 1989, ApJ, 344, 325
Larson, R. B. 1998, MNRAS, 301, 569
Li, W., Leaman, J., Chornock, R., et al. 2011, MNRAS, 412, 1441
Limongi, M., & Chieffi, A. 2018, ApJS, 237, 13
Lineweaver, C., Fenner, Y., & Gibson, B. 2004, Sci, 303, 59
Lucchesi, R., Jablonka, P., Skúladóttir, Á., et al. 2024, A&A, 686, A266
MacFadyen, A. I., & Woosley, S. E. 1999, ApJ, 524, 262
Mannucci, F., Della Valle, M., & Panagia, N. 2006, MNRAS, 370, 773
Matteucci, F., Panagia, N., Pipino, A., et al. 2006, MNRAS, 372, 265
McConnachie, A. W. 2012, AJ, 144, 4
Melott, A. L., & Thomas, B. C. 2011, AsBio, 11, 343
Mo, H. J., & White, S. D. M. 2002, MNRAS, 336, 112
Muñoz, R. R., Côté, P., Santana, F. A., et al. 2018, ApJ, 860, 66
Pace, A. B. 2024, arXiv:2411.07424
Pagnini, G., Salvadori, S., Rossi, M., et al. 2023, MNRAS, 521, 5699
Pancino, E., Romano, D., Tang, B., et al. 2017, A&A, 601, A112
Prantzos, N. 2008, SSRv, 135, 313
Raiteri, C. M., Villata, M., & Navarro, J. F. 1996, A&A, 315, 105
Rossi, M., Salvadori, S., Skúladóttir, Á., & Vanni, I. 2023, MNRAS, 522, L1
Ruderman, M. A. 1974, Sci, 184, 1079
Saccardi, A., Salvadori, S., D'Odorico, V., et al. 2023, ApJ, 948, 35
Salvadori, S., Skúladóttir, Á., & Tolstoy, E. 2015, MNRAS, 454, 1320
Salvadori, S., Tolstoy, E., Ferrara, A., & Zaroubi, S. 2014, MNRAS, 437, L26
Sigurdsson, S. 1992, ApJL, 399, L95
Simon, J. D. 2019, ARA&A, 57, 375
Spinelli, R., Ghirlanda, G., Haardt, F., Ghisellini, G., & Scuderi, G. 2021, A&A, 647, A41
Spitoni, E., Gioannini, L., & Matteucci, F. 2017, A&A, 605, A38
Spitoni, E., Matteucci, F., & Sozzetti, A. 2014, MNRAS, 440, 2588
Suda, T., Katsuta, Y., Yamada, S., et al. 2008, PASJ, 60, 1159
Testi, L., Natta, A., Manara, C. F., et al. 2022, A&A, 663, A98
Thomas, B. C., Jackman, C. H., Melott, A. L., et al. 2005a, ApJL, 622, L153
Thomas, B. C., Melott, A. L., Jackman, C. H., et al. 2005b, ApJ, 634, 509
Thorsett, S. E. 1995, ApJL, 444, L53
Todini, P., & Ferrara, A. 2001, MNRAS, 325, 726
Tolstoy, E., Hill, V., & Tosi, M. 2009, ARA&A, 47, 371
Tucker, W. H. 1981, in NASA Conf. Publication 2156, Life in the Universe, ed. J. Billingham (Cambridge, MA: MIT Press), 287
Vanni, I., Salvadori, S., Skúladóttir, Á., Rossi, M., & Koutsouridou, I. 2023, MNRAS, 526, 2620
Vorobyov, E. I., Whalen, D. J., Latif, M. A., et al. 2025, arXiv:2501.08375
Weisz, D. R., Dolphin, A. E., Skillman, E. D., et al. 2014, ApJ, 789, 147
Whalen, D. J., Latif, M. A., & Jessop, C. 2025, NatAs, 9, 741
Woosley, S. E., & Weaver, T. A. 1995, ApJS, 101, 181
Zink, J. K., Hardegree-Ullman, K. K., Christiansen, J. L., et al. 2023, AJ, 165, 262